Active tectonics in northern Victoria Land (Antarctica) inferred from the integration of GPS data and geologic setting

M. Dubbini,[1] P. Cianfarra,[2] G. Casula,[3] A. Capra,[4] and F. Salvini[2]

Received 10 November 2009; revised 2 August 2010; accepted 7 September 2010; published 24 December 2010.

[1] A semipermanent Global Positioning System (GPS) network of 30 vertices known as the Victoria Land Network for Deformation Control (VLNDEF) was set up in the Austral summer of 1998 in northern Victoria Land (NVL), including Terra Nova Bay (TNB), Antarctica. The locations were selected according to the known Cenozoic fault framework, which is characterized by a system of NW-SE regional faults with right-lateral, strike-slip kinematics. The TNB1 permanent GPS station is within the VLNDEF, and following its installation on a bedrock monument in October 1998, it has been recording almost continuously. The GPS network has been surveyed routinely every two summers, using high-quality, dual-frequency GPS receivers. In this study we present the results of a distributed session approach applied to the processing of the GPS data of the VLNDEF. An improved reference frame definition was implemented, including a new Euler pole, to compute the Antarctic intraplate residual velocities. The projection of the residual velocities on the main faults in NVL show present-day activities for some faults, including the Tucker, Leap Year, Lanterman, Aviator, and David faults, with right-lateral strike-slip kinematics and local extensional and compressional components. This active fault pattern divides NVL into eight rigid blocks, each characterized by its relative movements and rigid rotations. These show velocities of up to several millimeters per year, which are comparable to those predicted by plate tectonic theory at active plate margins.

Citation: Dubbini, M., P. Cianfarra, G. Casula, A. Capra, and F. Salvini (2010), Active tectonics in northern Victoria Land (Antarctica) inferred from the integration of GPS data and geologic setting, *J. Geophys. Res.*, *115*, B12421, doi:10.1029/2009JB007123.

1. Introduction

[2] The East Antarctic craton has long been considered a stable continent that is surrounded by passive margins [e.g., *Cande et al.*, 2000]. The tectonic setting of northern Victoria Land (NVL) contrasts with this picture. A set of NW-SE striking, regional faults cuts across NVL and connects to the fracture system of the Southern Ocean: the Balleny and Tasman Fracture zones [*Salvini et al.*, 1997; *Storti et al.*, 2007; *Faccenna et al.*, 2008]. Recent geologic investigations have shown that some of these faults were active in Upper Cenozoic time [*Di Vincenzo et al.*, 2004]. Furthermore, the pattern of the main glaciers in the region has been strongly influenced by these faults [*Salvini and Storti*, 1999]. The recent and active volcanoes along these glaciers and the seismic activity associated with them strongly suggest the presence of active tectonics in NVL. All of this neotectonic evidence favors the hypothesis that at least some of these faults are active.

[3] The use of space geodesy can provide the data required to define the role of the fault set within the present-day active tectonics of NVL. Over the last few years, enlargement of the GPS satellite system, improvements in the global continuous GPS tracking network, use of more sophisticated space vectors and atomic clocks, and rapid improvements in the Global Navigation Satellite System (GNSS) have all provided improvements to global plate-velocity site measurements, global reference-framework definitions, satellite orbits, and other global Earth-orientation parameters. At the same time, the establishment of several worldwide regional permanent and semipermanent networks of GPS stations has increased the number of stations available for linking various observations [*Serpelloni et al.*, 2006; *Casula et al.*, 2007]. In addition, the quality of the data from modern dual-frequency receivers has benefited from several technological improvements, including increases in the numbers of channels and in the internal memory.

[4] These systematic observations for spatial geodesy in Antarctica began during the Australian summer of 1990–1991 [*Capra et al.*, 2007] in the framework of the Scientific Committee on Antarctic Research (SCAR) surveys, to study the geodynamics of the area, to estimate the crustal deformation,

[1]Dipartimento di Discipline Storiche, Antropologiche e Geografiche, Università di Bologna, Bologna, Italy.
[2]Dipartimento di Scienze Geologiche, Università degli Studi di Roma Tre, Rome, Italy.
[3]Istituto Nazionale di Geofisica e Vulcanologia, Sezione di Bologna, Bologna, Italy.
[4]Dipartimento di Ingegneria Meccanica e Civile, Università di Modena e Reggio dell'Emilia, Modena, Italy.

0148-0227/10/2009JB007123

and to compute an improved reference frame [*Dietrich et al.*, 2001, 2004; *Manning et al.*, 2005]. Following these trends, within the Italian National Research Project in Antarctica, *Capra et al.* [1996] planned and realized the application of GPS technology and other geodetic facilities in NVL, East Antarctica.

[5] Since the 1998 Austral summer, geodetic infrastructures have been installed in the area of Terra Nova Bay (TNB), in NVL, East Antarctica. The semipermanent GPS network of the Victoria Land Network for Deformation Control (VLNDEF) consists of a total of 30 stations installed since the Austral summer of 1999–2000, and it was specifically designed with the aim of estimating crustal deformation in this region [*Capra et al.*, 2004, 2007]. At least four complete seasonal campaigns (1999, 2001, 2003, and 2007) and a set of continuous observations for the TNB1 permanent GPS site have been collected over this time span, from 1999 to the present.

[6] The aim of the present study is twofold: first, to publish the results obtained from the integrated processing of data in the VLNDEF GPS network and, second, to define the tectonic interpretation of these results in the active tectonic setting of NVL.

[7] A new definition of the Euler pole for Antarctica was computed and used to remove the inherently rigid rotation of the plate, so that intraplate velocities can be estimated for use as input observations for the tectonic interpretation of the NVL area. Our results show that some of the main regional faults that characterized NVL had significant movement along their segments over this observation period, and thus the kinematics found fully confirm that the reorganization of the plate tectonics that started in the late Oligocene period (approximately 40 Ma) in the Australia–Southern Ocean–East Antarctica system is still ruling the tectonics in NVL, with right-lateral, strike-slip, intraplate faulting with velocities comparable to those predicted at plate boundaries by plate tectonic theory.

2. Geologic and Geodynamic Setting

[8] The present-day geologic framework of NVL (Figure 1) is the result of long tectonic evolution that has been dominated by a system of NW-SE elongated faults; these have been intermittently active since the lowermost Paleozoic period [e.g., *Bradshaw et al.*, 1985; *Borg and Stump*, 1987; *GANOVEX Team*, 1987; *Kleinschmidt and Tessensohn*, 1987]. Previous studies have recognized that at least two of these faults (the Leap Year and Lanterman faults) represent the boundary between terranes that were juxtaposed during the Ross Orogeny in the Cambro-Ordovician period (about 480 Ma) [*GANOVEX Team*, 1987, and references therein]. Three major terranes have been identified: from the SW to the NE, the Wilson, Bowers, and Robertson Bay terranes.

[9] The outcrops of the Wilson Terrane are characterized by high to suborderly, low-grade metamorphic rocks of the Neoproterozoic to Early Paleozoic period, which are deeply intruded by granitoids of Granite Harbour intrusives (500–480 Ma [*Gunn and Warren*, 1962; *Borg and Stump*, 1987]).

[10] The Bowers Terrane consists of Cambrian low-grade, meta-volcanic, and meta-sedimentary rocks that are derived from an oceanic environment [e.g. *Weaver et al.*, 1984, and references therein]. Of note, the Lanterman Fault, which represents the boundary between these two terranes, is characterized by a belt of mafic to ultramafic rock with eclogites [*Ricci et al.*, 1996] and relatively limited overthrusts (Mt. Murchison Thrust), both of which testify to the strong activity of this fault during the juxtaposition.

[11] The Robertson Bay Terrane consists of a thick succession of very low grade metaturbidites of the Cambro-Ordovician period [*Wright et al.*, 1984]. The progressive peneplanation of the Ross Orogen produced a series of erosional surfaces up to the Permian and the sub-Beacon peneplains. During this process, in Devonian-Carboniferous time (350 Ma), a new tectonic event was responsible for a granitoid intrusion episode that almost exclusively involved the NE sector of NVL (i.e., the Robertson Bay and Bowers terranes). In Permo-Triassic time the deposition of sandstone and conglomerates of the Beacon Supergroup [*Barrett et al.*, 1972] confirmed that the peneplanation was complete. Continental deposition was followed in Jurassic time by tholeiitic magmatism (mostly volcanites), Ferrar dolerites, and Kirkpatrick basalts of the Ferrar Supergroup [*Grindley*, 1963]. This magmatic event is referred to as the initiation of the Australia–East Antarctica rifting, and it was followed in Cretaceous time by the development of a major faulting tectonic event. This latter resulted in the opening of the Ross Sea basin and initiation of drifting between Australia and East Antarctica. A series of what are today N-S oriented basins within the Ross Sea allows us to guess at the extension direction at that time. It is important to note here that at the initiation of and during the rifting process, the old regional sutures (the NW-SE fault system today) represented a series of correctly oriented corridors of crustal weakness, and they favored development of the transform faulting and fracture zones that are required for the plate tectonic geometry of the Australia–East Antarctica drifting. As a result, the main transforms (such as the Tasman and Balleny fracture zones) are located on offshore projections of the main NW-SE faults onshore (Figure 1).

[12] By its inherited character, the Australia–Southern Ocean–East Antarctic plate tectonic framework has been characterized by the presence of a series of weak corridors deeply inside the continental lithosphere in the Cenozoic [*Storti et al.*, 2007]. As expected, there is a similar evolution on the Australian projection of these fracture zones, both offshore and onshore, that is, the Newer Volcanic Province [*Lesti et al.*, 2008].

[13] The major plate tectonic reorganization and its acceleration in the South and Southern Pacific oceans that occurred during lowermost Late Cenozoic time (approximately 40 Ma) was eased by the reactivation along these weak corridors. This was thus responsible for the important right-lateral, strike-slip movements [*Wilson*, 1995; *Paulsen and Wilson*, 2004] that added their transform component in the Southern Ocean [*Salvini et al.*, 1997; *Rossetti et al.*, 2003]. If these additional components were too difficult to be separated from drifting in the oceanic crust, only the strike-slip component propagated onshore. The result was the development (or reactivation of inherited, weak corridors) of the NW-SE, right-lateral, strike-slip system in southern Victoria Land [*Wilson*, 1995] and NVL [*Salvini et al.*, 1997], as well as on the Australia side [*Lesti et al.*, 2008, and references therein]. A series of transtensional to

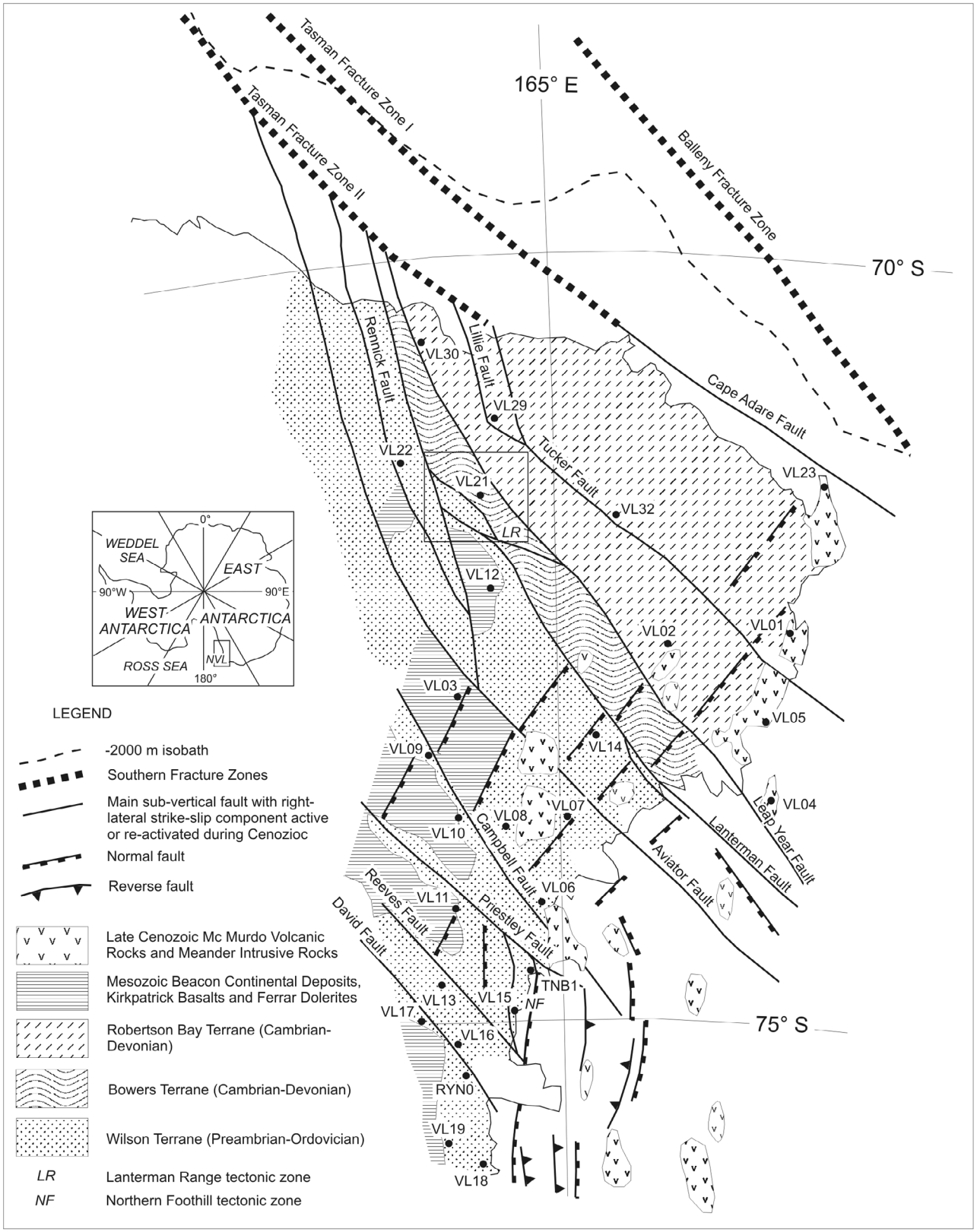

Figure 1. Cenozoic tectonic map of the northern Victoria Land (NVL) region, redrawn from *Salvini et al.* [1997], with the locations of the GPS network sites. The tectonic setting is characterized by a series of reactivated regional faults with right-lateral, strike-slip kinematics. Inset: Location within the map of Antarctica. The square marks the location of the area shown in Figure 2.

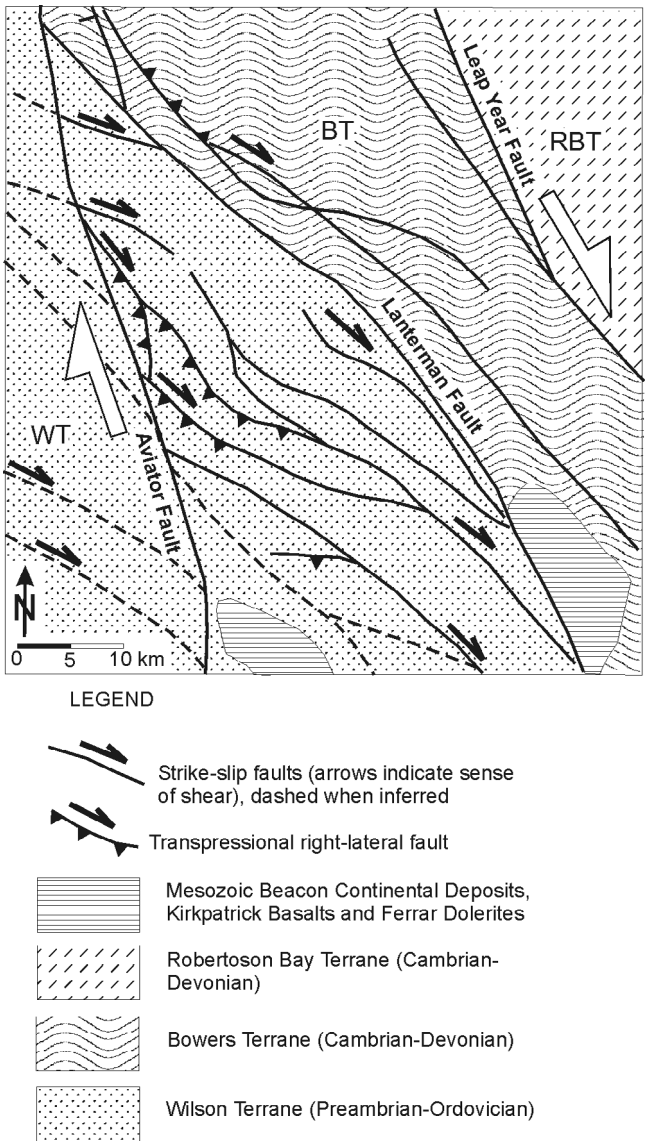

Figure 2. Structural map of the Lanterman Range area, modified from *Rossetti et al.* [2003] showing the transpression and reverse faulting associated with the main right-lateral, strike-slip motion along the Aviator and Lanterman faults. Refer to Figure 1 for location.

extensional N-S basins is associated with the right-lateral, strike-slip regime; this series is produced by interactions between adjacent NW-SE faults that merge into the Ross Sea rifting region to the SE. (Re-)activation of this fault system and its interaction with the E-W extension have resulted in the development of tholeiitic volcanism, which is characterized by the development of central volcanoes at the correct intersection of the main NW-SE faults, with the N-S normal faults in between, for example, Mt. Melbourne Volcano [*Salvini et al.*, 1997; *Salvini and Storti*, 1999].

[14] Whether the Late Cenozoic tectonics are still active at present in NVL is an open debate, although the age of the volcanism and the glacier path following the NW-SE pattern, which exactly matches the main faults, provide a strong suggestion of recent activity [*Salvini and Storti*, 1999].

[15] Investigations into the Lanterman Range area (Figure 2) have indicated that right-lateral, strike-slip motion is associated with local transpression and reverse faulting with a brittle character along the western side of the Lanterman Range, facing the Lanterman Fault [*GANOVEX Team*, 1987; *Roland and Tessensohn*, 1987]. Apatite fission track analyses have confirmed a late Paleogene age (38 Ma) for the start of the last uplifting episode, confirming the activity age of the Lanterman Fault [*Rossetti et al.*, 2003].

3. Victoria Land Network for Deformation Control Data and the GPS Campaigns

[16] Since the establishment of the Geodetic Infrastructure in Antarctica (GIANT) project in the framework of the SCAR international program in 1992, and with the supervision of Antarctic Neo-Tectonics, a committee of specialists, there has been a geodesy program with the following objectives.

[17] 1. Creation of a common geodetic reference frame for all of the scientists in Antarctica.

[18] 2. Global geodetic contributions based on the definition of the terrestrial-geodetic reference frame.

[19] 3. Monitoring services for the crustal deformations, in terms of horizontal and vertical movements.

[20] Useful measures have been realized through different techniques: very-long-baseline interferometry; Doppler orbitography, and radiopositioning integrated by satellite, absolute gravity, tide gauges; and GNSS [*Capra et al.*, 2008]. In 1995 a series of periodic GPS measurement campaigns, the SCAR GPS Epoch Project, was started, which was coordinated by R. Dietrich of the T.U. Dresden (Germany), with the aim of defining and maintaining the GPS Antarctic network within the International Terrestrial Reference Frame (ITRF). Following these measurement campaigns, the first permanent geodetic GPS observatories were established in Antarctica. Three years later, in 1998, in the framework of the GIANT program of SCAR, the Italian permanent geodetic observatory (ITRF code TNB1) was established in Antarctica, near the Mario Zucchelli Station (MZS) of the Italian scientific base in the area of TNB. In the period from 1999 to 2001 the VLNDEF geodetic network was finally created (Figure 1).

[21] All of these infrastructures take part in the international activities of the Polar Earth Observing Network consortium, which is particularly interested in dynamic knowledge of the polar areas and installation of permanent observatories. The main purpose of the VLNDEF is to detect neotectonic phenomena within the area of NVL and to provide metric parameters for the definition of glacial isostatic adjustment models. For these reasons, particular attention has been paid to site choice and benchmark materialization.

[22] The TNB1 permanent GPS station is a part of the VLNDEF, and it is equipped with an ASHTECH Z-XII-III receiver and an ASH700936 Dorne Margolin antenna, with a SNOW radome established by means of a reinforced concrete pillar anchored directly to a granitic outcrop. All of the instruments are contained inside a controlled-temperature, thermally isolated shelter. Since the distance between TNB1 and MZS is approximately 600 m, and since

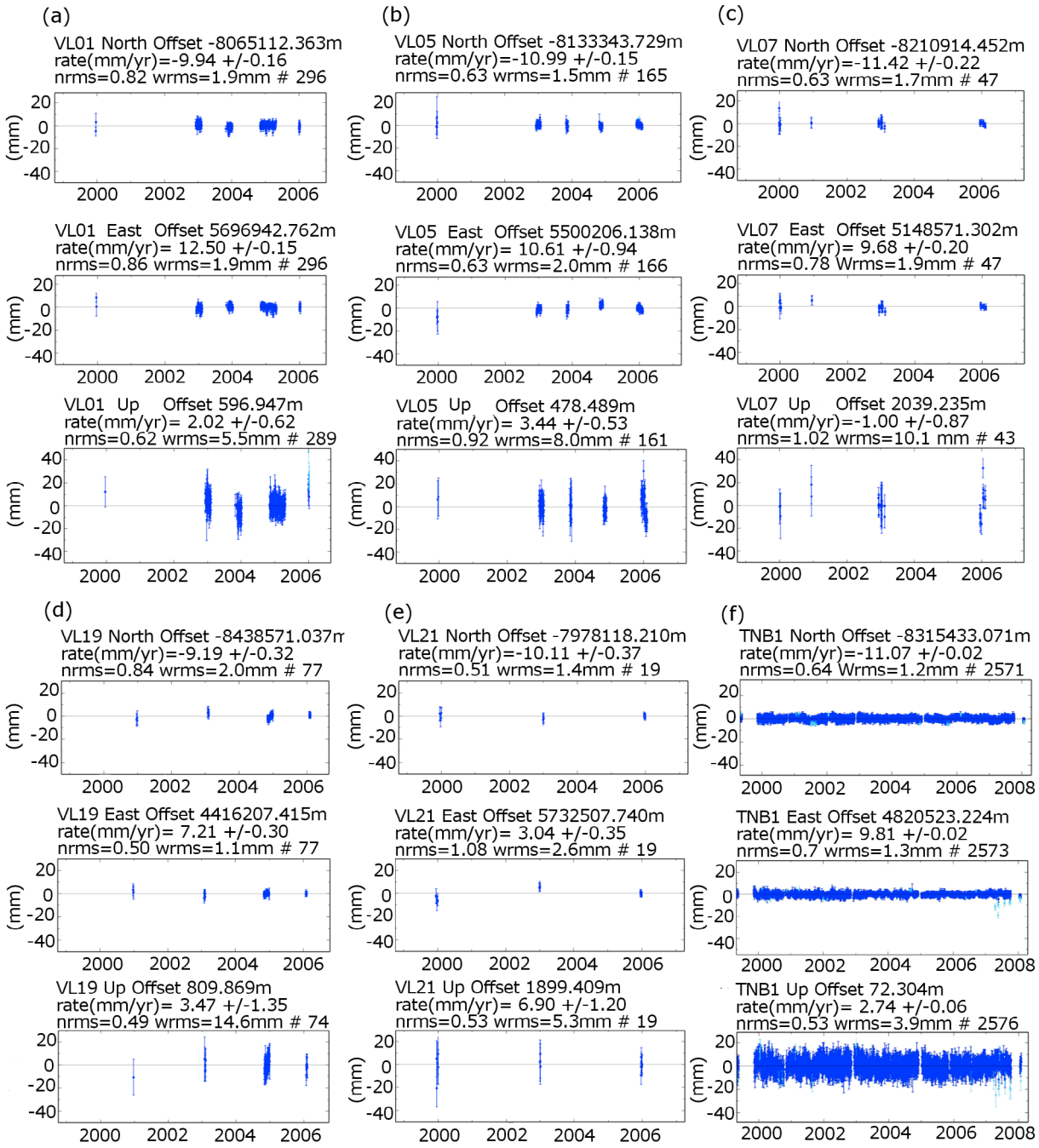

Figure 3. (a–e) Victoria Land Network for Deformation Control (VLNDEF) nonpermanent and (f) TNB1 permanent GPS sites displacement time series. North, east, and vertical components are represented in sequence. Values represent deviations from trend.

TNB1 is a permanent GPS station with continuous data acquisition, a direct cable connection to electrical power at the MZS base was established, 24 h per day, 365 days per year. Data recorded at TNB1 are saved daily to a hard disk device inside the MZS station, which is directly connected to a GPS receiver by modem, with a yearly download for processing the data during seasonal Italian scientific expeditions. The typology of the construction has provided evidence of very high stability at the site, considering the results of a time series analysis of the data (Figure 3).

[23] Other benchmarks of the VLNDEF have been defined, by considering that the GPS campaigns should be held periodically, with the purpose of minimizing errors due to antenna height measurements. Following these indications, we decided to install a benchmark comprising a stainless-steel pillar firmly anchored to the rock outcrops, with a 5/8 inch screw at the top, which made it possible to screw the choke-ring antenna directly to the benchmark itself.

[24] With the aim of defining a dynamic tectonic model of NVL, the choice of the network benchmark site was deter-

Table 1. Victoria Land Network for Deformation Control (VLNDEF) Nonpermanent Stations for the Number of Daily Sessions per Site During These Antarctic Campaigns

	Antarctic Campaign					
Site	1999–2000	2000–2001	2002–2003	2003–2004	2004–2005	2005–2006
VL01	2		57	55	170	12
VL02	8		36			13
VL03	9		16			22
VL04			4	18		5
VL05	5		50	17	35	65
VL06		1	7	8	35	17
VL07	8	2	21			17
VL08	4	2	9			13
VL09	10		19			13
VL10	8		25		36	44
VL11	3	1	9			17
VL12	8		31	29	69	62
VL13	4	5	11			13
VL14	12		20	26	36	52
VL15		6	11	8		7
VL16		8	14		12	13
VL17		7	17	9	46	13
VL18		4	10		7	13
VL19		4	8		53	11
VL20	2		4			
VL21	5		4			10
VL22	6		7			9
VL23				40	20	6
VL24						6
VL25						9
VL27	1		7			
VL29	4	5				11
VL30	2		5			5
VL32	2		15			22

mined on the basis of the Cenozoic tectonics derived from previous geologic studies [*Salvini et al.*, 1997]. Other fundamental logistics were also taken into account, such as the presence of stable outcrops, the full visibility of the sky, and the possibility of accessing the site through landing of a helicopter. The VLNDEF spans an area that extends for approximately 700 km in the N-S direction and approximately 300 km in the E-W direction, with a mean distance between sites of roughly 60 km (Figure 1).

[25] In the southern part of NVL the VLNDEF partially overlaps with the TransAntarctic Mountains Deformation Network, which was established by Ohio State University and the U.S. Geological Survey for studying crustal deformation and tectonic settings in the area of southern Victoria Land [*Willis et al.*, 2006; *Wilson et al.*, 1999].

[26] Since the establishment of VLNDEF in 1999, six periodic GNSS measurement campaigns have been undertaken (Table 1). During each campaign, different types of instruments and antennas have been used (e.g., Trimble, Ashtech, Topcon). Simultaneous acquisitions have been performed by dividing the overall network into clusters, with the aid of daily sessions, with cutoff angles of 10^{o} and a 15 s data-acquisition rate.

4. GPS Data Analysis and Methodology

4.1. General Description

[27] GPS measurements in the VLNDEF have been carried out with two tasks in mind: (i) to obtain information regarding the movement of the Antarctic plate with respect to the Pacific plate, by improving our knowledge of the position and velocity of the rotation pole; and (ii) to estimate intraplate movements in the area of NVL more precisely.

[28] To accomplish these tasks, we used a set of redundant GPS measurements taken from the Antarctic and peri-Antarctic stations over a time span of approximately 7 years, together with GPS observations of nonpermanent sites. Additionally, GPS observations performed using the VLNDEF vertices were carried out annually, and sometimes biannually (i.e., 1999–2000, 2000–2001, 2002–2003, 2003–2004, 2004–2005, 2005–2006), using daily sessions for a period of at least 10 continuous days (Table 1). The simultaneous recordings of at least seven GPS receivers per day provided a particularly effective application for data processing. The main problem during GPS data processing for an Antarctic network (i.e., VLNDEF) is a loss of connection of these dense nonpermanent stations to the network and to the peri-Antarctic stations located in Oceania, Africa, and South America; because of the extreme flexibility of the distributed-sessions approach, this problem has been solved. As determined from the literature [*Dong et al.*, 1998; *Serpelloni et al.*, 2006; *Casula et al.*, 2007], such a strategy is based on the creation of daily loose-constraint solutions, called quasi-observations (h-files), by means of the GAMIT/GLOBK 10.3 modules of the Massachusetts Institute of Technology [*Herring et al.*, 2006a, 2006b] and by involving in these solutions both the nonpermanent stations of the VLNDEF and some Antarctic and peri-Antarctic stations of the VLNDEF and International GNSS Service (IGS).

[29] In the following steps the observations were computed by means of a robust combination of quasi-observations,

using solutions computed by other analysis centers, like the Scripps Orbit and Permanent Array Center (http://garner.ucsd.edu). The process consisted of using solutions (quasi-observations) obtained using precise orbits and solutions with at least two or three permanent, common stations. At this stage stochastic model consistency was verified by evaluation of the stochastic parameter χ^2, which was used to weight the observations. During the third and final step the adjustments of the combined solutions were determined, together with their stabilization and georeferring in the global ITRF2005 [*Altamimi et al.*, 2007]. Using this approach, it was possible to remove the rigid rotation of the plate using a general definition of the Euler vector, which represents the rotation of the Antarctic Plate with respect to the Pacific Plate. This was given by *Altamimi et al.* [2007] for global determination of the ITRF2005.

4.2. GPS Data Processing Strategy

[30] As stated, the GPS data processing was performed using the GAMIT/GLOBK software (version 10.3) developed at the Harvard Smithsonian Center of Astrophysics, Massachusetts Institute of Technology, and the Scripps Institution of Oceanography, University of California, San Diego. This software is composed of several routines for GPS processing and data modeling that are sequentially applied following different steps, with the aid of Unix c-shell facilities. At the beginning, double-differenced, iono-free combinations were used to compute loosely constrained daily solutions with coordinates, orbits, atmospheric delays, integer ambiguities, and variance-covariance matrices.

[31] Owing to the nonlinear nature of the equation-related observables, an iterative procedure was used to improve the coordinate solutions by applying a weighted least-squares algorithm at least twice. With this approach, the residuals were reduced from centimeters to millimeters. Cycle slips were detected and repaired or removed using a cleaning tool for observable automatic editing. Ambiguities of double differences were solved using the Melbourne-Webbena wide-lane linear phase-code combination. The IGS precise orbits were used. Other dynamic models were initially considered: the default gravitational field IGS/International Earth Rotation and Reference Systems Service (IERS) 1992 model [*McCarthy*, 1996] and the nongravitational acceleration of satellites model [*Colombo*, 1986; *Beutler*, 1994].

[32] Atmospheric gradients and zenith delays were estimated to consider the effects of azimuthal asymmetry, using a piecewise linear function over the observation time period. The default models for the dry and wet components of atmospheric delays were used in a subsequent step, as described by *Saastamoinen* [1972]. The a priori model adopted for zenith delay correction was the global pressure and temperature model developed by *Boehm et al.* [2006a]. This model is based on the fit of spherical harmonics to meteorological data, and it generated surface pressure and temperature values as a function of location and time. In particular, we used site-by-site values of zenith delay corrections, extrapolated from a global grid a priori file generated by the Vienna mapping function [*Boehm et al.*, 2006b].

[33] Because of the mixed antenna-receiver types used in this network, we used the new (2006–2007) absolute phase center corrections of satellite and receiver antennas. The ionosphere contribution was greatly reduced through the use of iono-free linear combinations, and it was modeled and stochastically adjusted. The IERS/IGS 2003 models for diurnal, semidiurnal, and terdiurnal solid earth tides [*McCarthy and Petit*, 2004] were determined, and pole-tide corrections were applied according to the IERS standards [*Dong et al.*, 2002; *Herring et al.*, 2006]. The ocean-loading tide effect was modeled using the FES2004 tide model produced at Centre National d'Etudes Spatiales [*Lyard et al.*, 2006].

4.3. Solution Editing and Error Analyses

[34] Data preprocessing was operated through the tsview facility using the GAMIT/GLOBK package [*Herring*, 2003] to estimate gross sources of errors, such as outliers and offsets. The output of the tsview package was suitably formatted and used as input for the GLOBK package. To obtain more realistic error ellipses (for semipermanent GPS sites), we took into account the time-correlated sources of errors using the global Kalman filter [*Casula et al.*, 2007].

[35] In the literature several approaches have been developed to account for the noise of GPS time series [*Mao et al.*, 1999; *Dixon et al.*, 2000; *Mazzotti et al.*, 2003; *McClusky et al.*, 2000, 2003; *Williams et al.*, 2003; *Reilinger et al.*, 2006; *Williams*, 2008]. As is well known, the position time series of data on permanent GPS sites are influenced by noise that can be described in the frequency domain as a power-law function with a spectral index k that varies between 0.5 and 2.0 [*Williams*, 2003]. By using this approach, we identified three components [*Mao et al.*, 1999]: a white noise with $k = 0$ and, for instance, no frequency dependence; a flicker noise with $k = -1$, which was Gaussian and depended on the period of some natural phenomena, such as atmospheric seasonal effects and orbital or tidal disturbances; and random-walk noise with a spectral index of $k = -2$, which was generally neglected, but was largely due to the monuments, and was sometimes seen after approximately 2 years of recordings. According to the literature, it is clear that a better estimate of noise in the GPS position time series has been reflected in more realistic error ellipses of the velocity field. In the present study we used different approaches to account for errors in the GPS time series. These included the Herring tsview real σ option of robust fit; the *Mao et al.* [1999] approach, using the formulas of *Dixon et al.* [2000] and *Mazzotti et al.* [2003]; and finally, the Create and Analyze Time Series (CATS) package [*Williams et al.*, 2004; *Williams*, 2008], with a noise power law of $k = 0.2$ applied to the TNB1 continuous GPS station, to account for the correct levels of noise. For the latter case we found that the error ellipses obtained with the GLOBK package were comparable with estimates of the CATS package, which uses the maximum likelihood method (Table 3, Figure 3).

5. Discussion

5.1. Reference Frame Definition

[36] To define the internal constraints for our solutions, we used data from seven Antarctic IGS permanent GPS

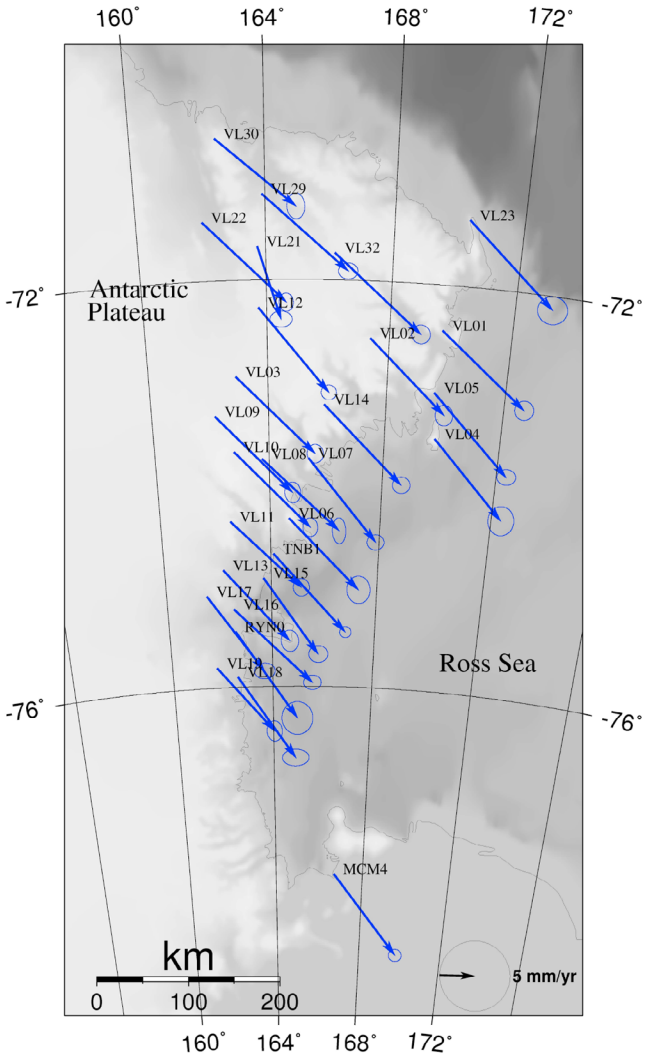

Figure 4. Absolute horizontal velocity vectors (mm/yr) for the 2005 International Terrestrial Reference Frame (ITRF), calculated at each site of the VLNDEF, with their associated error ellipses; 95% confidence ellipses, 2σ.

stations, four Antarctic permanent GPS stations belonging to the TransAntarctic Mountains Deformation Network project, and seven peri-Antarctic permanent GPS stations belonging to the IGS global network. The loosely constrained daily estimates for station coordinates (h-files) were successively aligned into ITRF2005 [*Altamimi et al.*, 2002, 2007] using a Helmert transformation.

[37] A distributed session approach (similar to sequential least-squares minimization) using sequential Kalman filtering was applied (considering the χ^2 parameter) to estimate the level of data fitting [*McClusky et al.*, 2000, 2003; *Reilinger et al.*, 2006]. Finally, the total adjusted solution was obtained in terms of coordinates and velocities, and daily coordinate estimates were given in the same reference frame (ITRF2005). The resulting horizontal absolute velocities are shown in Figure 4, with the 95% confidence ellipses [*Wessel and Smith*, 1998]. Obviously, neither the definition of the Nuvel-1A [*Argus and Gordon*, 1991] nor the general definition of the Euler pole given by *Altamimi et al.* [2007] in the ITRF2005 was sufficient to completely remove the inherent rigid rotation of the Antarctic plate from the GPS site velocity field. For these reasons we estimated a Euler pole with the aid of the plate tool of the GLOBK package, to best fit and correct the rotation of the Antarctic plate and to invert the intraplate residual velocity field of the VLNDEF.

[38] To infer rigid motion of the plate we defined the Antarctic plate by choosing nine of the more stable IGS permanent GPS stations. This was based on their intraplate residual velocities, which were obtained by a preliminary computation that used the rotation rate defined by the Altamimi ITRF2005 Euler pole and were negligible (<1 mm/yr) (Figure 5). In the following step we ran the GLOBK facility to estimate the intraplate VLDEF GPS site velocities, as well as the positions and rotation rates of the Euler pole (Table 2).

5.2. Intraplate Horizontal Velocities

[39] Residual horizontal velocities were obtained from the absolute velocities by removing the previously determined rotation, and they are shown in Figure 6. Most of the values were between 0 and 2 mm/yr, with the exception of the VL21 site. The error ellipses at the 95% confidence level were computed with the aid of the GLOBK 10.3 package, taking into account the white and colored noise (red and pink), and they were comparable with those computed with the Mao formula [*Mao et al.*, 1999] and those with errors obtained by applying the CATS package to the permanent GPS station time series [*Williams*, 2008].

[40] In general, we can confirm that in the most optimistic of cases (e.g., a permanent site operating continuously for over 5 years), an error (1σ) can be obtained that is of the order of 0.2 mm/yr for the horizontal component and 0.7 mm/yr for the vertical component (Table 3).

5.3. Vertical Velocities

[41] As shown in Figure 7 the vertical velocities were generally positive and ranged between 0 and 4 mm/yr. Despite the improvements in atmospheric modeling used in the GAMIT processing, the velocities fell within the estimated errors, as can be seen by analyzing the time series of the permanent and nonpermanent GPS sites (e.g., Figures 3a–3f). Indeed, the weighted root mean square errors obtained by applying a robust fit to the longest time data series (TNB1) showed a reduction from 6 to 4 mm/yr in the vertical component after atmospheric modeling improvements (application of the Vienna mapping function [*Boehm et al.*, 2006b]). Table 3 reports the velocity data of station TNB1 computed by fitting the three-component position time series over a time span of 7 years, with the aid of different algorithms.

6. Active Tectonics of Northern Victoria Land

6.1. Methodology

[42] The spatial distribution of the residual horizontal velocities (Figure 6) showed strong variability, resulting in a puzzling strain-rate field for the investigated area. In contrast, higher local differences in residual velocities between neighboring stations were located in sectors where geologic studies have shown evidence of intense Meso-Cenozoic tectonic activity, namely, the Lanterman Range and the Northern Foothills (Figures 1 and 2) [*Roland and Tessensohn*,

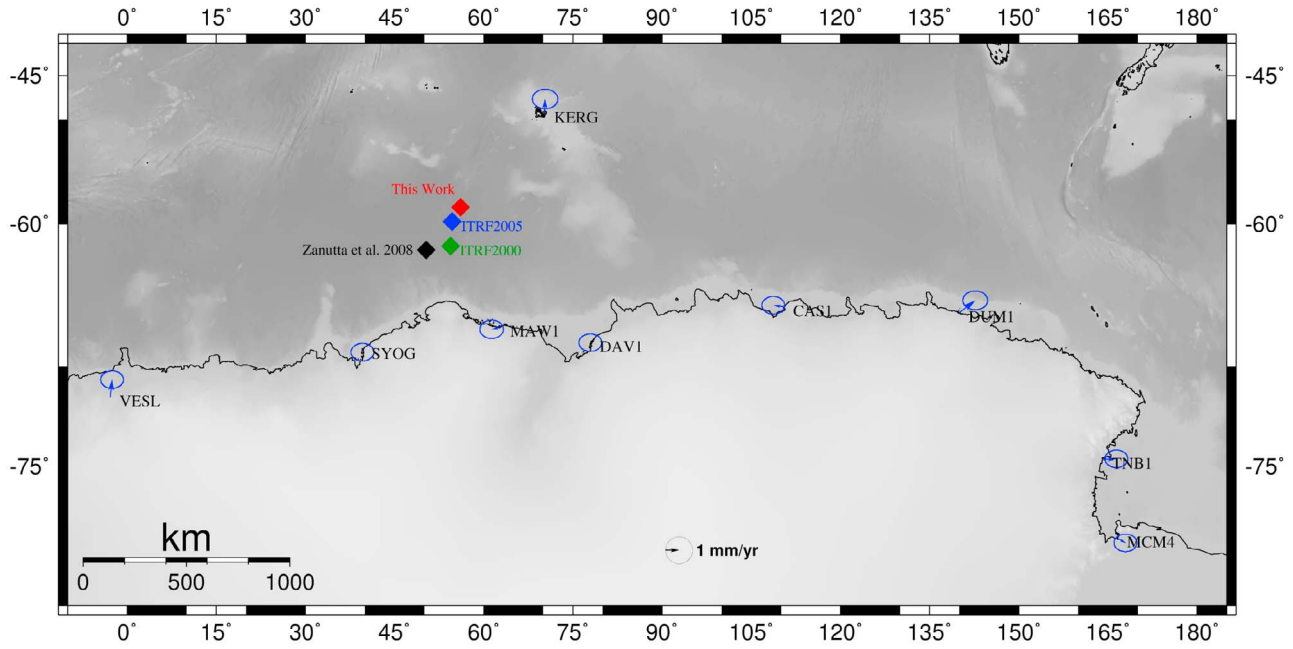

Figure 5. Positions for the Euler poles of rotation, calculated in different studies; our estimate of the Euler pole (red) was computed using data registered at the sites marked.

1987; *Skinner*, 1987; *Salvini et al.*, 1997; *Rossetti et al.*, 2003]. This evidence suggested a framework for computing the residual velocity field into a block tectonic model using the Cenozoic regional fault set on NVL, that is, the same set that was used to organize the GPS network (Figure 8). The results of this comparison confirmed the compatibility of the velocity pattern found with the block model, including present-day activity for some of the NW-SE regional faults. Computed residual horizontal velocities for each GPS station (i.e., subtracting the clockwise rotation of the Antarctic plate, approximately 2.21×10^{-6} rad, surrounding a Euleran pole at 58.6°S, 56.0°E; see Table 2) were projected along the neighboring regional faults. The projection was carried out with the assumption that there are rigid-block tectonics in NVL and that the deformation and relative movements are confined within the block margins corresponding to the fault segments.

[43] Only pairs of GPS stations lying on opposite sides of a given fault were selected, as this was the only fault between them. The tectonic model used assumed that the strain was concentrated on the faults. In this way the relative velocities found corresponded to the fault velocities. These velocities would represent the resulting combination of relative rigid block motion and strain accumulation at block boundaries, rather then mere actual fault slips. Since most of the stations were located far enough from the faults, this assumption is reasonable. In contrast, strain distribution has been reported across regional strike-slip faults (e.g., San Andreas Fault [*Turcotte and Schubert*, 2002]), with an increasing strain rate approaching the fault and, therefore, a decreasing cumulative relative displacement between pairs of points closer to the fault. Four GPS stations, namely, VL09, VL10, VL29, and VL30 (Figure 8), were located close enough to the studied faults to represent this situation. In this case the computed relative displacements would represent a fraction of the total displacement between the blocks. Accordingly, the displacement velocities found represented a conservative hypothesis for the present-day block-fault activity in NVL.

[44] Projected vectors were split into their along-strike and across-strike fault components. The comparison of these components for each pair of GPS stations located on opposite sides of the faults considered allowed the computation of the strike-slip and the extensional and shortening components of the relative velocities between adjacent blocks. The computation was carried out by adding the modules of the analyzed components for vectors trending in the opposite sense and by subtracting the modules for the vector with the same sense (see Table 5). Resulting values

Table 2. Relative Euler Poles[a]

Model	Latitude (°N)	Longitude (°E)	ω (deg/Myr)
Dietrich et al. [2004]	−63.000 ±1.000	54.700 ±6.000	0.221 ±0.014
ITRF2000	−61.830 ±2.143	54.426 ±3.689	0.231 ±0.015
ITRF2005	−59.813 ±0.864	54.685 ±1.676	0.223 ±0.007
Zanutta et al. [2008]	−62.110 ±0.925	50.280 ±1.276	0.228 ±0.004
Present study	−58.586 ±2.152	56.077 ±2.419	0.221 ±0.008

[a]ITRF, International Terrestrial Reference Frame. Euler poles computed in the present study compared with those reported by *Dietrich et al.* [2004] and *Zanutta et al.* [2008] and with the absolute determinations of Euler poles given by *Altamimi et al.* [2002, 2007] for ITRF2000 and ITRF2005, respectively.

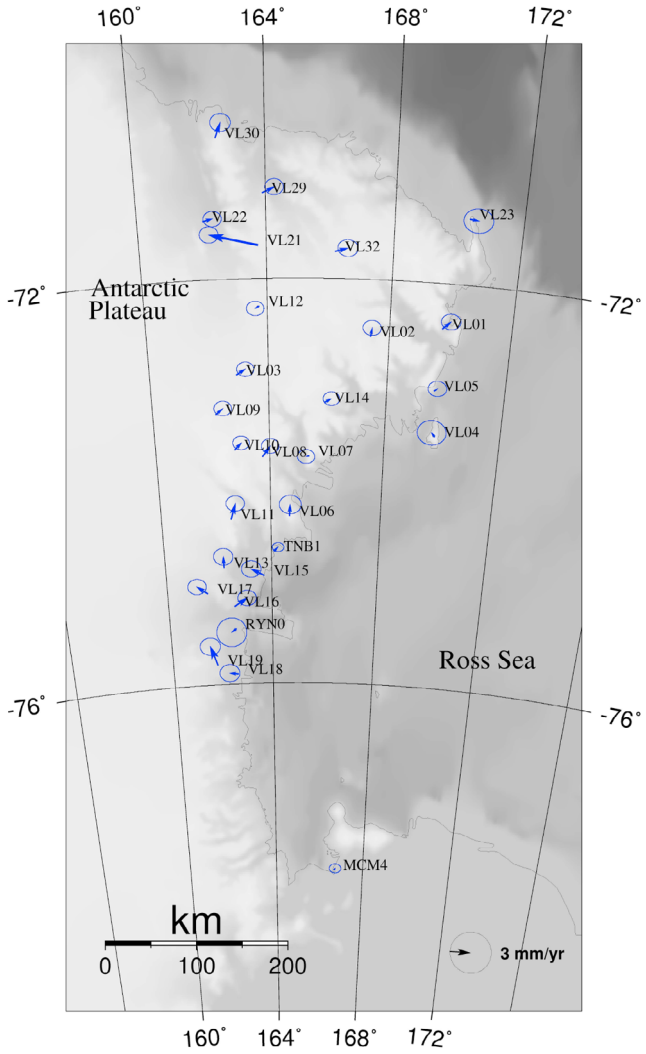

Figure 6. Residuals of the horizontal velocity vectors (mm/yr) for the ITRF2005, calculated at each site of the VLNDEF, with their associated error ellipses; 95% confidence ellipses, 2σ.

greater than 1 mm/yr were considered meaningful for the present analysis. The overall picture of the displacement velocities found showed a general right-lateral strike-slip movement of the fault network, locally associated with transtensional or transpressional components.

[45] The VL21 GPS station represents a single NW residual component. This might result from monument instability, although this hypothesis cannot be considered realistic, owing to the particular Antarctic climatic conditions characterized by permanent-freeze conditions. The GPS sites were preliminary surveyed by geologists of the Italian National Research Project in Antarctica team. The analysis allowed us to identify the fault segments that were active during the recorded time interval (Figure 8).

[46] A comparison of the residual velocity vectors of the VL21 and the VL22 GPS stations showed a left-lateral shear component of 6.9 mm/yr and a 4.7 mm/yr shortening along the Lanterman Fault in the area of the Lanterman Range. In the northernmost sector of the Leap Year Fault, NE of the Lanterman Range, there was a right-lateral shear of 5.1 mm/yr, with an associated extension of 5.9 mm/yr, as shown by the comparison between the VL21 and the VL30 stations. Along the Tucker Fault the velocity vector comparison between the GPS station pairs VL32-VL02 and VL01-VL02 showed right-lateral strike-slip movements of 2.2 and 1.4 mm/yr, respectively. The VL05-VL01 pairing showed an extension of 1 mm/yr in the coastal segment of this fault. The Lillie Fault was characterized by a right-lateral motion of 1.8 mm/yr, as shown by the velocity vectors of VL30 and VL29. A comparison of the residual velocities of the VL03 and VL14 stations indicated that there was no significant relative motion in the NW sector of the Aviator Fault. There was an extension of 1.4 mm/yr for its coastal sector, as indicated by the VL07-VL14 comparison. The Priestley Fault had no significant motion (i.e., it was <1 mm/yr), as derived from the VL10-VL11 pairing.

[47] Higher velocity values characterized the coastal zone between the Priestley Fault and the Reeves Fault, for the area including the Northern Foothills (where TNB and the MZS were located) and Inexpressible Island (Figure 1). The comparisons between station pairs VL11-TNB1 and VL11-VL15 indicated that there was an active fault, which links the Priestley Fault to the Reeves Fault along the western border of this block. The comparison between TNB1 and VL11 showed a 1.3 mm/yr right-lateral, strike-slip motion in the northern sector. The central sector of this fault had no meaningful right-lateral motion (0.9 mm/yr), which was associated with a shortening of up to 2.6 mm/yr (VL11-VL15). The Reeves Fault was characterized by no significant motion, as indicated by the comparison between the VL11 and the VL13 stations. The contrasts between station pairs VL13-VL17 and VL16-RYN0 along the David Fault in the NE sector showed a right-lateral strike-slip motion with a velocity of 0.9 mm/yr, with an associated relative extension of 1.4 mm/yr along its northwestern sector and 2.7 mm/yr to the SE.

[48] The comparisons among the residual motions of stations VL03, VL06, VL08, VL09, and VL10 indicated that the Campbell Fault did not show significant relative motion during the observation period. Similar results characterized the northern segment of the Aviator Fault and the Rennick Fault, as shown by a comparison between the VL03 and the VL22 stations.

[49] Comparison of the GPS stations VL18 and VL19 south of the David Fault showed evidence of relative motion between them (Figure 8). No faults have been proposed in this sector, although if we assumed the presence of a fault parallel to the David Fault, we derived an along-strike, right-lateral velocity of 1.1 mm/yr associated with a larger

Table 3. Comparison Among the Estimated ITRF2005 Velocities for the TNB1 Permanent GPS Station in the ITRF2005[a]

TNB1, ITRF2005	$V_e/\sigma V_e$ (mm/yr)	$V_n/\sigma V_n$ (mm/yr)	$V_u/\sigma V_u$ (mm/yr)
GLOBK 5.15	9.97 ±0.22	−11.16 ±0.22	1.91 ±0.71
tsview 2.00 R/F	9.79 ±0.03	−11.03 ±0.04	2.65 ±0.10
Enfit/Mao/Dixon R/F	9.81 ±0.40	−11.06 ±0.40	2.58 ±1.41
Enfit/Mao/Mazzotti R/F	9.81 ±0.28	−11.06 ±0.18	2.58 ±1.20
CATS MLE 3.1.2	9.80 ±0.21	−10.97 ±0.20	3.05 ±0.62

[a]CATS, Create and Analyze Time Series; TNB, Terra Nova Bay; V_e, east velocity; V_n, north velocity; V_u, uplift velocity. Thirty-nine percent confidence ellipses, 1σ. See text for explanation.

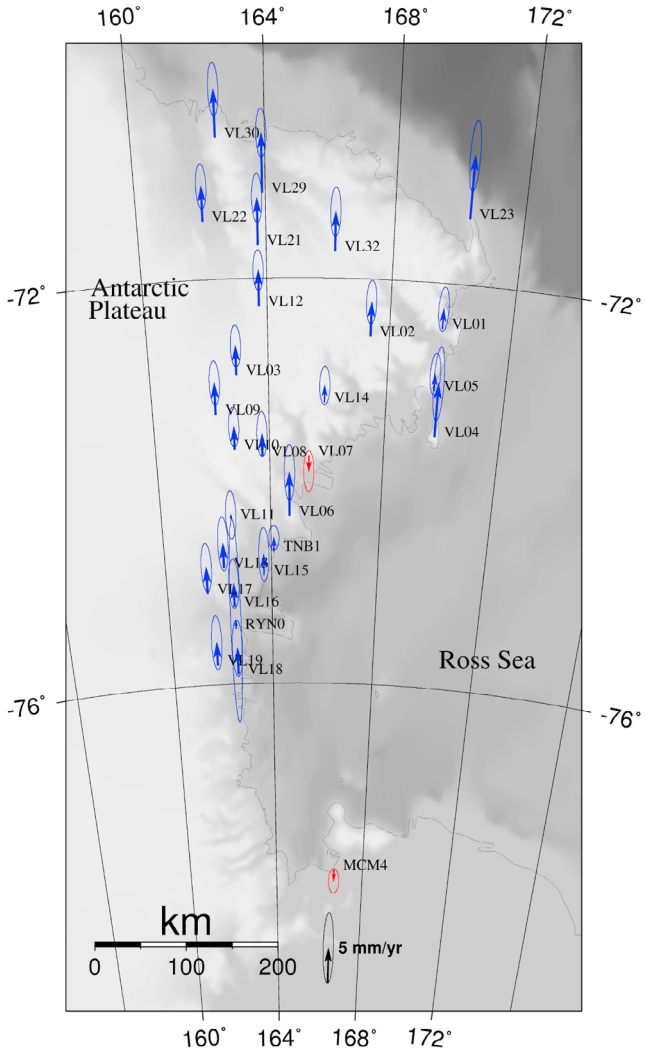

Figure 7. Vertical velocity vectors (mm/yr) calculated at each site of the VLNDEF, with their associated error ellipses; 95% confidence level, 2σ. For graphical representation reasons, only the semimajor axis should be considered.

transpressional component of 2.4 mm/yr. These proposed components would be fully compatible with the general framework found.

6.2. Tectonic Framework

[50] Results from the projection of the GPS showed that some fault segments are active (Table 5). The GPS network was not sufficient to constrain all of the faults in the tectonic model, yet it was sufficient to constrain the active or locked character of many of the fault segments (Figure 8).

[51] Displacements were found along portions of the Tucker, Leap Year, Lanterman, Aviator, and David faults (Figure 8). In contrast, the GPS evidence showed that, at least for the observed periods, there were no significant displacements along the Rennick, Campbell, Priestley, and Reeves faults. The latter two faults showed relative movement values just below the 1 mm/yr threshold used, and their connection with the active Northern Foothills Fault leaves open the hypothesis of limited activity.

[52] The onshore GPS network could not resolve motions along the Cape Adare offshore fault, and no definitive results were found for the NW segment of the Tucker Fault. The GPS network results were not sufficient for detecting movement along SE segments of the Lanterman and Leap Year faults, although the small differences in motion among stations across these segments strongly suggested that the movements, if present, would have been negligible over the observed decade.

[53] The active faults dissected NVL into five main tectonic blocks, namely, from north to south, the Victory, Rennick, Mesa, Nansen, and Larsen blocks. Two smaller blocks, the Lanterman and the Northern Foothills blocks, were also seen and were characterized by higher displacement rates (Figure 9). Althogh the resulting velocities within each block are relatively homogeneous, as can be deduced by comparing values from Table 4, the presence of rotations reduces the reliability of using a variance analysis to characterize block rigidity (Table 5).

[54] The SE sector of the Tucker Fault was characterized by right-lateral, strike-slip displacement with a velocity of between 0.3 and 2.1 mm/yr. An extensional component was also present in the southeasternmost sector of the fault, with values of extension of up to 1 mm/yr. Right-lateral, strike-slip displacement with a velocity of 1.8 mm/yr was seen for the Lillie Fault, where no component orthogonal to the fault segment was seen.

[55] The Leap Year Fault showed evidence of intense activity along its NW segment. The segment of the Leap Year Fault NE of the Lanterman Range had one of the largest observed displacements. The right-lateral, strike-slip component reached a velocity higher than 5 mm/yr, and was associated with an extensional velocity of approximately 6 mm/yr, which gives a transtensional, right-lateral overall displacement velocity of approximately 8 mm/yr for this fault segment. To the SE this fault did not show clear evidence of activity, although constraints from the GPS network do not allow a definitive result.

[56] The Lanterman Fault showed evidence of important activity in its NNW-SSE segment bordering the Lanterman Range. There the velocity computed by the GPS measures showed a left-lateral, strike-slip displacement with a velocity higher than 6.9 mm/yr, associated with a shortening velocity of 5.7 mm/yr. These data contrast with those measured along the segment of the Leap Year Fault on the opposite side of the Lanterman Range. Two geological models may need to be proposed to solve this puzzle. The apparent opposite displacements might be the result of block rotation tectonics [*Beck*, 1989; *McKenzie and Jackson*, 1989]. Owing to the relatively low strength of rocks under extensional regimes, stress conditions between pairs of synthetic faults can easily induce the dissection of the region confined between faults into a series of blocks, through the initial development of extensional faulting. These blocks are free to rotate synthetically to ease the strike-slip motion, and this rotation can induce antithetic movements along the newly created faults (i.e., the formerly extensional faults). The relative rotation of these blocks would produce an opposite symmetry of compression and extension along their border, depending on the sense of rotation. Within this model the velocity pattern observed for the Lanterman Range can be solved with a clockwise rotation of the Lanterman Block. In

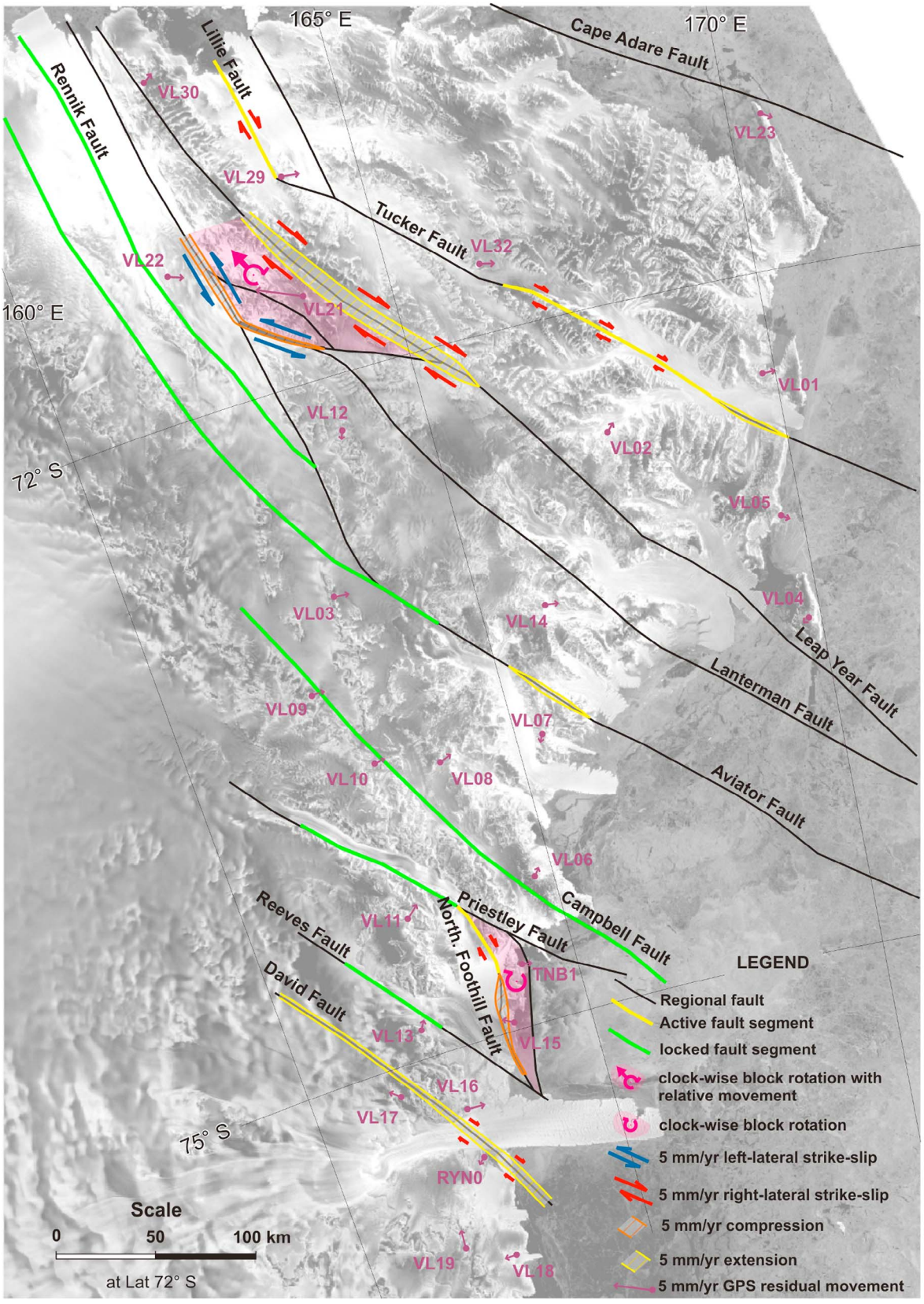

Figure 8. Horizontal residual velocities projected along the main Cenozoic faults in NVL assuming block tectonic kinematics. This allowed us to identify the fault segments that were active during the recording time interval (1998–2008), which were characterized by strike-slip kinematics with local transpression or transtension components. The background image is a subset of the Radarsat mosaic of Antarctica.

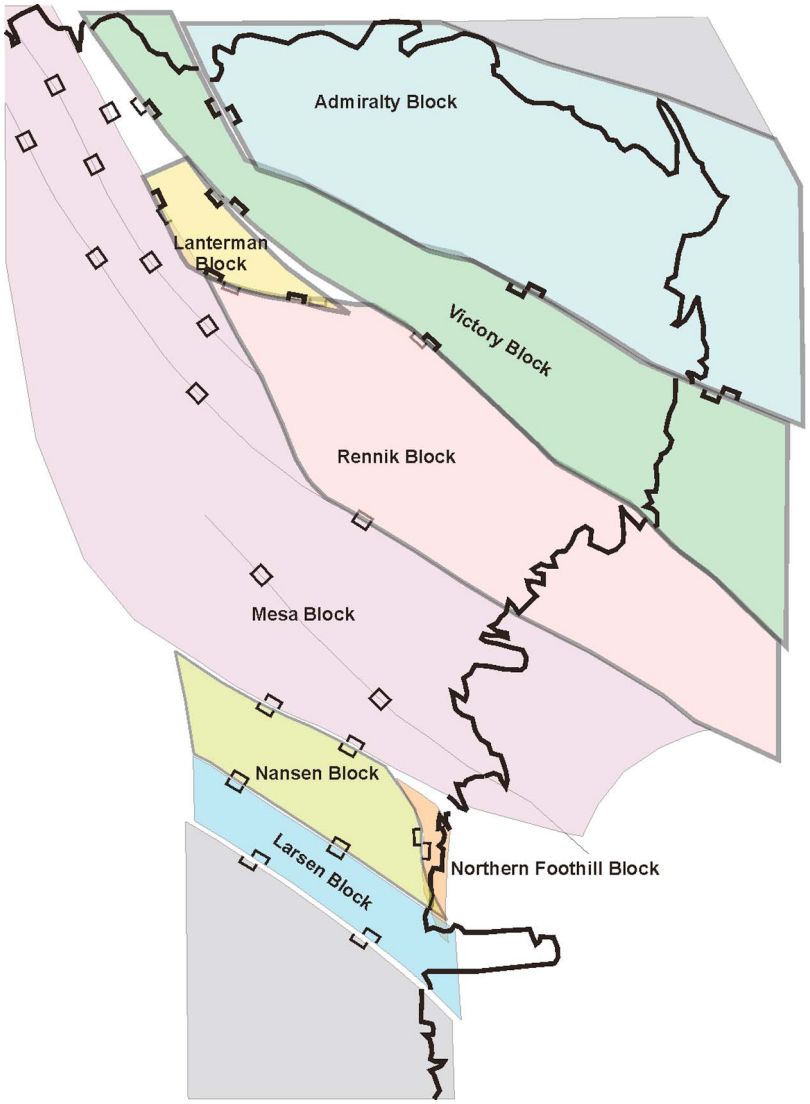

Figure 9. Sketch map showing the eight rigid crustal blocks dissected out by the active fault network in NVL during the recording time. The block displacements are exaggerated and scaled to measured horizontal residual velocities (see Figure 8). Split and unsplit squares are superimposed on the main faults to show their relative offsets.

contrast, the combination of left-lateral and right-lateral motions on the sides of the Lanterman Range may well be the result of a relative translation of this block toward the NW, due to strong transpressional conditions. These two hypotheses may well partly coexist. In this area the movements shown largely agree with results from the field geology [*GANOVEX Team*, 1987; *Rossetti et al.*, 2003] (Figure 2). The western side of the Lanterman Range shows a series of NNW-SSE striking thrusts that have been active since 40 Ma [*Rossetti et al.*, 2003]. Field investigations revealed that almost all of the strike-slip faults had a right-lateral sense of motion, in contrast to the left-lateral motion seen by GPS measurements. A reasonable explanation of this is that the Lanterman Range block is located in a restraining bend of the Lanterman Fault, and it suffers from shortening tectonics, while block tectonics (i.e., rotation) started more recently than the age of the exposed faults (about 40 Ma). In this way the evolution of the block would be slightly different from that of a tectonic block developed initially as a transpressional deformation. Offsets along the main fault were responsible for the relative movement of the block, compatible with the general right-lateral motion, toward the SE. As the Lanterman Block reached the restraining bend zone of the branching of the Lanterman Fault from the Aviator Fault, it was compelled to rotate clockwise (i.e., compatible with the general motion). This rotation was responsible for the collision of the WSW border against the Lanterman Fault and the consequent shortening associated with the persistence of the thrusts. Translation of this block to the NNW might be produced by the relative motion of the Leap Year, Lanterman, and Aviator faults.

[57] The motions described remain confined to the Lanterman Block, since GPS showed that the Rennick Fault had no significant motion over this last decade, confirming

Table 4. Velocities of the VLNDEF GPS Station and the Permanent GPS Stations Involved in the Computation (TNB1, MCM4) in the ITRF2005 Reference Frame[a]

Site	Long. (deg)	Lat. (deg)	V_e, ITRF2005 (mm/yr)	V_n, ITRF2005 (mm/yr)	V_e, Intraplate (mm/yr)	V_n, Intraplate (mm/yr)	σV_e (±mm/yr)	σV_n (±mm/yr)	Correlation Factor (rad)	V_u (mm/yr)	σV_u (±mm/yr)
MCM4	166.669	−77.838	8.95	−11.23	0.42	−0.30	0.37	0.36	−0.002	−1.57	0.71
RYN0	162.571	−75.454	8.25	−12.47	−0.52	−0.80	0.89	0.95	0.007	1.17	5.90
TNB1	164.103	−74.699	9.97	−11.16	0.91	0.07	0.33	0.32	−0.004	1.91	0.71
VL01	169.725	−72.45	12.38	−10.30	1.64	0.51	0.55	0.56	0.011	2.80	1.30
VL02	167.378	−72.565	10.85	−10.46	0.62	1.00	0.51	0.60	−0.005	4.86	1.27
VL03	162.926	−72.951	10.86	−11.13	1.61	0.43	0.47	0.54	0.00	4.11	1.22
VL04	169.749	−73.518	10.22	−10.78	−0.09	−0.10	0.75	0.85	−0.001	7.55	2.17
VL05	169.612	−73.063	11.04	−11.11	0.83	−0.24	0.55	0.45	0.018	2.31	1.21
VL06	164.691	−74.35	9.74	−10.11	0.41	0.98	0.67	0.80	−0.003	6.14	1.62
VL07	165.379	−73.76	9.55	−11.78	−0.04	−0.61	0.49	0.44	0.005	−2.19	1.20
VL08	163.74	−73.764	10.71	−10.31	1.49	1.14	0.39	0.75	−0.001	3.21	1.32
VL09	162.169	−73.331	10.48	−11.17	1.39	0.42	0.46	0.60	−0.002	4.45	1.29
VL10	162.769	−73.688	10.41	−10.96	1.31	0.60	0.43	0.54	−0.003	3.25	1.17
VL11	162.542	−74.371	9.66	−9.61	0.98	1.64	0.47	0.51	−0.005	0.60	1.40
VL12	163.727	−72.274	9.72	−12.14	−0.02	−0.82	0.44	0.43	−0.010	5.08	1.18
VL13	162.205	−74.848	8.95	−10.30	0.25	1.03	0.50	0.62	−0.019	3.40	1.58
VL14	165.906	−73.228	11.04	−11.21	1.33	0.18	0.51	0.48	0.001	2.37	1.12
VL15	163.716	−74.934	7.49	−10.87	−1.50	0.36	0.55	0.49	−0.001	2.95	1.57
VL16	162.545	−75.233	10.67	−10.69	2.11	0.57	0.51	0.42	−0.003	3.22	1.43
VL17	161.539	−75.095	7.55	−10.92	−1.28	0.47	0.60	0.46	−0.001	3.73	1.41
VL18	162.594	−75.899	7.72	−11.66	−1.17	−0.41	0.77	0.48	−0.002	3.65	1.63
VL19	161.782	−75.805	7.65	−9.22	−0.59	2.18	0.44	0.59	−0.001	3.20	1.57
VL21	163.733	−71.669	3.17	−10.38	−6.49	1.00	0.64	0.47	−0.003	6.64	1.43
VL22	162.04	−71.422	11.40	−11.71	1.79	−0.09	0.41	0.53	0.004	4.99	1.32
VL23	170.305	−71.346	12.71	−11.60	1.62	−0.62	0.87	0.81	0.002	9.03	2.08
VL29	163.896	−71.154	12.09	−11.09	2.14	0.34	0.56	0.47	0.001	8.49	1.43
VL30	162.525	−70.599	11.19	−9.91	1.23	1.86	0.52	0.76	−0.003	6.91	1.57
VL32	166.165	−71.733	12.40	−11.26	2.21	0.02	0.54	0.54	−0.018	5.60	1.44

[a]Thirty-nine percent confidence ellipses, 1σ (i.e., 2.44 is the conversion factor from 1σ to 2σ).

the proposed model of NNW relative translation of the Lanterman Block and the prevailing present-day transpression in the area. Similar results characterize the Aviator Fault, where the GPS relative motion indicated that the fault was locked to the NW and showed an extension of 1.4 mm/yr in its SE segment. The Campbell Fault also appeared to be locked, based on results from comparisons among several GPS stations. Evidence of right-lateral, transtensional motion was also found along the southernmost faults of NVL, on the David Fault, with values of up to 2.7 mm/yr. The Priestley Fault showed a possible right-lateral, transpressional motion along the Priestley Glacier, with a right-lateral strike-slip component rate of 0.8 mm/yr and a shortening rate of 0.7 mm/yr.

Table 5. Fault Movements as Derived From the Projections of Residual Velocities of the GPS Station Pairs[a]

Fault	Reference Fault Strike	GPS Station Pair	Along-Strike Relative Velocity (mm/yr)	Across-Strike Converging Velocity (mm/yr)	Fault Movement Type
Tucker	N120°	VL32-VL02	2.189	(<0.2)	Right-lateral
Tucker	N119°	VL01-VL02	1.394	(<0.2)	Right-lateral
Tucker	N117°	VL01-VL05	(0.328)	−1.037	Transtensional
Lillie	N155°	VL29-VL30	1.762	(<0.2)	Right-lateral
Leap Year	N133°	VL30-VL21	5.060	−5.894	Right-lateral transtensional
Lanterman	N132°	VL21-VL22	−6.882	4.731	Left-lateral transpressional
Lanterman	N99°	VL21-VL12	−6.675	(0.786)	Left-lateral
Rennik	N142°	VL22-VL03	(0.521)	(<0.2)	Locked
Aviator	N122°	VL03-VL14	(<0.2)	(0.360)	Locked
Aviator	N125°	VL14-VL07	(0.669)	−1.433	Transtensional
Campbell	N137°	VL03-VL09	(<0.2)	(<0.2)	Locked
Campbell	N135°	VL08-VL10	(−0.255)	(−0.51)	Locked
Priestley	N120°	VL10-VL11	(0.806)	(0.736)	Possibly locked
Northern Foothills	N151°	TNB1-VL11	1.339	(0.822)	Right-lateral
Northern Foothills	N172°	VL11-VL15	(0.922)	2.634	Transpressional
Reeves	N126°	VL11-VL13	(0.232)	(−0.923)	Possibly locked?
David	N126°	VL13-VL17	(0.909)	−1.352	Transtensional
David	N128°	VL16-RYN0	1.229	−2.699	Right-lateral transtensional

[a]Positive (negative) values indicate right (left)-lateral and compressional (extensional) movements. Values in parentheses are below the 1 mm/yr reliability threshold used.

[58] The velocities measured at stations surrounding the Northern Foothills Block presented a puzzle similar to that described for the Lanterman Block, with the western border showing extension of less than 1 mm/yr in the northern sector, which inverted in the southern sector, where shortening reached values of up to 2.6 mm/yr. The strike-slip component along this border of the Northern Foothill Block was approximately 1.3 mm/yr to the north, where it reached a compressional component of 0.8 mm/yr. Strike-slip motion decreased to 0.2 mm/yr to the SW. In this case the presence of block rotation tectonics might well justify the found motions. The Reeves Fault showed a lower velocity, with no strike-slip motion and an extensional rate that was limited to 0.9 mm/yr. The David Fault had a transtensional motion, with a right-lateral, strike-slip velocity of about 1 mm/yr, associated with an extension rate of 1.3–2.7 mm/yr. The resulting total relative displacement rate along this fault was approximately 3.6 mm/yr.

[59] Seismic activity in NVL confirms the active tectonic framework observed. Since the 1960s a number of earthquakes have been reported in this region [*Reading*, 2002]. This activity might well represent the results of elastic stress accumulation along the active fault segments found (Figure 8). A temporary broadband seismometer array was positioned in Austral summer 1999–2000 in the central trans-Antarctic Mountains and showed fault-related seismic activity along the David Fault [*Bannister and Kennett*, 2002].

[60] As indicated in the foregoing geologic and geodynamic setting details, the NW-SE trending Cenozoic faults of NVL are the onshore extension of two fracture zones of the Southern Ocean, namely, Tasman Fracture Zones I and II (Figure 1). These fracture zones have accommodated the rifting and drifting between East Antarctica and Australia. The presence of high seismic activity [*Storti et al.*, 2007] along their active segments (the zones separating the two riftings, following classical plate tectonic theory) shows evidence of extra strike-slip motion. Evidence of Quaternary activity in the northern projection of these fracture zones was found for the Australian continent, with the presence of the tectonovolcanic Newer Volcanic Province [*Lesti et al.*, 2008].

[61] The relative horizontal displacement seen along some of the NW-SE regional faults in NVL might well be the intracontinental extension of this right-lateral, strike-slip motion as it splits and fades into the extensional tectonics in the Ross Sea. The relative horizontal displacement rate observed, which was of the order of millimeters per yeear, is comparable to the velocities predicted between adjacent plates by plate tectonic theory. In this way the Tasman Fracture Zones not only are a classic transform fault of the Southern Ocean expansion [*Wilson*, 1965], but also might also represent an active, incipient, plate boundary.

[62] The vertical velocities (Figure 7) showed the general uplift of NVL, although most of the reported uplift was well within the measurement uncertainty. These movements might relate to recent ice loss in the region. Uplift related to ice loss has been seen in the Arctic region [e.g., *Jiang et al.*, 2010]. As discussed by *Bevis et al.* [2009], with the present-day data set available for NVL, caution should be taken in attributing the vertical movements to mere glacial rebound, owing to the difficulties in separating this from the tectonic components.

7. Conclusions

[63] GPS measurements have proven here to be a useful tool for highlighting the geodynamics and neotectonics of NVL through the detection of crustal deformation. The proposed strategy of data processing has successfully allowed reduction of the error, thus revealing movements of the order of a few centimeters over a decade of observation. With use of this method, nonpermanent-station residual velocity errors are quite comparable with those from permanent stations. The final intraplate residual velocities obtained allowed us to recognize the main tectonic faults and their velocity trends in the VLNDEF area. With better constraint of the Euler pole, they absolute measured velocities confirm the clockwise (rigid) rotation of the East Antarctic Plate.

[64] These data confirm the tectonic activity of NVL and the primary role of the regional fault set. The present-day fault motions agree well with the Upper Cenozoic tectonic framework, thus confirming the long-lasting activities of these faults and their framework in the regional geodynamics of the Australia–Southern Ocean–East Antarctica plate system. The Tucker, Leap Year, Lanterman, Aviator, and David faults are active today and are characterized by right-lateral, strike-slip kinematics with a subordered local component of extension/compression.

[65] The Lanterman Range and Northern Foothills areas showed intense relative movements, with local rigid rotation that matched their complex tectonic setting. The intracratonic velocity field measured is comparable to the velocity predicted by plate tectonic theory at active margins and confirms the present-day active tectonic role of the Balleny and Tasman fracture zones, which propagate into the East Antarctic craton through its continental "passive margin."

[66] Future improvements will include increasing the numbers of semipermanent GPS stations of VLNDEF and the availability of GPS transects across the more active faults. Maintenance and exploitation of the Italian geodetic infrastructures in NVL are of great interest to the entire Antarctic scientific community.

[67] **Acknowledgments.** All research was carried out in the framework of the Programma Nazionale di Ricerche in Antartide (PNRA) and financially supported by PNRA S.C.r.l. The authors wish to acknowledge the two anonymous reviewers, whose suggestions greatly improved the quality of the paper.

References

Altamimi, Z., P. Sillard, and C. Boucher (2002), ITRF2000: A new release of the International Terrestrial Reference Frame for Earth science applications. *J. Geophys. Res.*, *107*(B10), 2214, doi:10.1029/2001JB000561.

Altamimi, Z., X. Collilieux, J. Legrand, B. Garayt, and C. Boucher (2007), ITRF2005: A new release of the International Terrestrial Reference Frame based on time series of station positions and Earth orientation parameters, *J. Geophys. Res.*, *112*, B09401, doi:10.1029/2007JB004949.

Argus, D., and R. Gordon (1991), No-Net Rotational model of current plate velocities incorporating plate motion model NUVEL-1, *Geophys. Res. Lett.*, *18*(11), 2039–2042.

Bannister, S. C., and B. L. N. Kennett (2002), Seismic activity in the Transantarctic Mountains: Results from a broadband array deployment, *Terra Antarct.*, *9*(1), 41–46.

Barrett, P. J., G. W. Grindley, and P. N. Webb (1972), The Beacon Supergroup of East Antarctica, in *Antarctic Geology and Geophysics*, edited by R. J. Adie, pp. 319–332, Universitetsforslaget, Oslo, Norway.

Beck, M. E. (1989), Block rotation in continental crust: examples from Western North America, in *Paleomagnetic Rotations and Continental Deformation*, edited by C. Kissel and C. Laj, pp. 1–16, Kluwer Academic Publishers.

Beutler, G., E. Brockmann, W. Gurtner, U. Hugentobler, L. Mervart, and M. Rothacher (1994), Extended orbit modeling techniques at the CODE Processing Center of the International GPS Service for Geodynamics (IGS): Theory and initial results, *Manuscr. Geod.*, *19*, 367–386.

Bevis, M., E. Kendrick, R. Smalley, I. Dalziel, D. Caccamise, I. Sasgen, M. Helsen, F.W. Taylor, H. Zhou, A. Brown, D. Raleigh, M. Willis, T. Wilson, and S. Konfal (2009), Geodetic measurements of vertical crustal velocity in West Antarctica and the implications for ice mass balance, *Geochem. Geophys. Geosyst.*, *10*, Q10005, doi:10.1029/2009GC002642.

Boehm, J., A. Niell, P. Tregoning, and H. Schuh (2006a), Global Mapping Function (GMF): A new empirical mapping function based on numerical weather model data, *Geophys. Res. Lett.*, *33*, L07304, doi:10.1029/2005GL025546.

Boehm, J., B. Werl, and H. Schuh (2006b), Troposphere mapping functions for GPS and very long baseline interferometry from European Centre for Medium-Range Weather Forecasts operational analysis data, *J. Geophys. Res.*, *111*, B02406, doi:10.1029/2005JB003629.

Borg, S. G., and E. Stump (1987), Early Paleozoic magmatism and associated tectonic problems of northern Victoria Land, Antarctica: Some problems and constraints, in *Gondwana Six: Structure, Tectonics, and Geophysics*, *Geophys. Monogr. Ser.*, vol. 40, edited by G. D. M. McKenzie, pp. 67–76, AGU, Washington, D. C.

Bradshaw, J. D., S. D. Weaver, and M. G. Lair (1985), Suspect terrances and Cambrian tectonics in northern Victoria Land, Antarctica, in *Tectonostratigraphic Terranes of Circum-Pacific Region*, *Earth Sci. Ser.*, vol. 1, edited by J. Howell, pp. 467–479, Circum-Pacific Research Council, Houston, Tex.

Cande, S. C., J. M. Stock, R. D. Müller, and T. Ishihara (2000), Cenozoic motion between East and West Antarctica, *Nature*, *404*, 145–150.

Capra, A., A. Gubellini, F. Radicioni, and L. Vittuari (1996), Italian Geodetic activities in Antarctica, in *Italian Geophysical Observatories in Antarctica*, edited by A. Meloni and A. Morelli, pp. 2–20, Compositori, Bologna, Italy.

Capra, A., S. Gandolfi, F. Mancini, M. Negusini, P. Sarti, and L. Vittuari (2004), Terra Nova Bay GPS permanent station, in *Terra Antartica Reports*, vol. 9, edited by G. Brancolini, C. Ghezzo, and A. Morelli, pp. 21–24, Terra Antart., Siena, Italy.

Capra, A., F. Mancini, and M. Negusini (2007), GPS, a geodetic tool for geodynamics in northern Victoria Land, Antarctica, *Antarct. Sci.*, *19*(1), 107–114.

Capra, A., M. Dubbini, A. Galeandro, L. Gusella, A. Zanutta, G. Casula, M. Negusini, L. Vittuari, P. Sarti, F. Mancini, S. Gandolfi, M. Montaguti, and G. Bitelli (2008), in *Geodetic and Geophysical Observations in Antarctica*, edited by A. Capra and R. Dietrich, pp. 37–72, Springer-Verlag, Berlin.

Casula, G., M. Dubbini, and A. Galeandro (2007), Modeling environmental bias and computing velocity field from data of Terra Nova Bay GPS network in Antarctica by means of a quasi-observation processing approach, in *Antarctica: A Keystone in a Changing World—Online Proceedings of the 10th ISAES*, edited by A. K. Cooper et al., *U.S. Geol. Surv. Open File Rep.*, *2007-1047*, 1–4, doi:10.3133/of2007-1047.srp054.

Colombo, O. L. (1986), Ephemeris errors of GPS satellites, *Bull. Geodes.*, *60*, 64–84.

D'Agostino, N., S. Mantenuto, E. D'Anastasio, A. Avallone, M. Barchi, C. Collettini, F. Radicioni, A. Stoppini, and G. Fastellini (2008), Contemporary crustal extension in the Umbria-Marche Apennines from regional CGPS networks and comparison between geodetic and seismic deformation, *Tectonophysics*, *476*(1–2), 3–12, doi:10.1016/j.tecto.2008.09.033.

Dietrich, R., et al. (2001), ITRF coordinates and plate velocities from repeated GPS campaigns in Antarctica-an analysis based on different individual solutions, *J. Geod.*, *74*, 756–766.

Dietrich, R., A. Rülke, J. Ihde, K. Lindner, H. Miller, W. Niemeier, H. W. Schenke, and G. Seeber (2004), Plate kinematics and deformation status of the Antarctic Peninsula based on GPS, *Global Planet. Change*, *42*(1–4), 313–321.

Di Vincenzo, G., S. Rocchi, F. Rossetti, and F. Storti (2004), 40Ar – 39Ar dating of pseudotachylytes: The effect of clast-hosted extraneous argon in Cenozoic fault-generated friction melts from the West Antarctic Rift System, *Earth Planet. Sci. Lett.*, *223*, 349–364.

Dixon, T. H., M. Miller, F. Farina, H. Wang, and D. Johnson (2000), Present-day motion of the Sierra Nevada block and some tectonic implications for the Basin and Range province, North American Cordillera, *Tectonics*, *19*(1), 1–24.

Dong, D. N., T. A. Herring, and R. W. King (1998), Estimating regional deformation from a combination of space and terrestrial geodetic data, *J. Geod.*, *72*, 200–214.

Dong, D., P. Fang, Y. Bock, M. K. Cheng, and S. Miyazaki (2002), Anatomy of apparent seasonal variations from GPS-derived site position time series, *J. Geophys. Res.*, *107*(B4), 2075, doi:10.1029/2001JB000573.

Donnellan, A., and B. P Luyendyk (2004), GPS evidence for a coherent Antarctic plate and for postglacial rebound in Marie Byrd Land, *Global Planet. Change*, *42*, 305–311.

Faccenna, C., F. Rossetti, T. W. Becker, S. Danesi, and A. Morelli (2008), Recent extension driven by mantle upwelling beneath the Admiralty Mountains (East Antarctica), *Tectonics*, *27*, TC4015, doi:10.1029/2007TC002197.

GANOVEX Team (1987), Geological map of the northern Victoria Land, Antarctica, 1:500000. Explanatory notes. *Geol. Jarbh.*, *66*, 779.

Grindley, G. W. (1963), The geology of the Queen Alexandra Range, Beardmore Glacier, Ross Dependency, with notes on the correlation of Godwana sequences, *N.Z. J. Geol. Geophys.*, *6*, 307–347.

Gunn, B. M., and G. Warren (1962), Geology of Victoria Land between the Mawson and Mulock glaciers, Antarctica, *N.Z. Geol. Surv. Bull. 71*, 157 pp.

Herring, T. A. (2003), MATLAB tools for viewing GPS velocities and time series, *GPS Solut.*, *7*(3), 194–199.

Herring, T. A., R. W King, and S. C. McClusky (2006a), *GPS Analysis at MIT, GAMIT Reference Manual*, *Release 10.3*, 91 pp., Dep. of Earth, Atmos., and Planet. Sci. Mass. Inst. of Technol., Cambridge.

Herring, T. A., R. W. King, and S. C. McClusky (2006b), *Global Kalman Filter VLBI and GPS Analysis Program, GLOBK Reference Manual*, *Release 10.3*, 182 pp., Dep. of Earth, Atmos., and Planet. Sci., Mass. Inst. of Technol., Cambridge.

Jiang, Y., T. H. Dixon, and S. Wdowinski (2010), Accelerating uplift in the North Atlantic region as an indicator of ice loss, *Nat. Geosci.*, *3*, 404–407.

Kleinschmidt, G., and F. Tessensohn (1987), Early Paleozoic westward directed subduction at the Pacific margin of Antarctica, in *Gondwana Six: Structure, Tectonics and Geophysics*, *AGU Geophys. Monogr. Ser.*, vol. 40, edited by G. D. McKenzie, pp. 89–105, AGU, Washington, D. C.

Lesti, C., G. Giordano, F. Salvini, and R. Cas (2008), Volcano-tectonic setting of the intraplate, Pliocene–Holocene, Newer Volcanic Province (Southeast Australia): Role of crustal fracture zones, *J. Geophys. Res.*, *113*, B07407, doi:10.1029/2007JB005110.

Lyard, F., F. Lefevre, T. Letellier, and O. Francis (2006), Modelling the global ocean tides: insights frpm FES2004, *Ocean Dynam.*, *56*, 394–415.

Mancini, F., A. Capra, S. Gandolfi, P. Sarti, and L. Vittuari (2004), VLNDEF (Victoria Land Network for DEFormation control). Monumentation during the GANOVEX VIII–ItaliaAntartide XV: Survey and data processing, *Terra Antarct.*, *11*(1), 35–38.

Manning, J. (2005), The evolution of the GIANT program, Report of Fifth Antarctic Geodesy Symposium, *SCAR Rep.*, *23*, 1–6.

Mao, A., G. Cristopher, A. Harrison, and T. H. Dixon (1999), Noise in GPS coordinate time series, *J. Geophys. Res.*, *104*(B4), 2797–2816.

Mazzotti, S., H. Dragert, J. Henton, M. Schmidt, R. D. Hyndman, T. S. James, Y. Lu, and M. Craymer (2003), Current tectonics of northern Cascadia from a decade of GPS measurements, *J. Geophys. Res.*, *108*(B12), 2554, doi:10.1029/2003JB002653.

McCarthy, D. D. (1996), *IERS Conventions 1996*, *IERS Tech. Note 21*, Obs. de Paris, Paris.

McCarthy, D. D., and G. Petit (2004), *IERS Conventions 2003*, *IERS Tech. Note 32*, Verlag des Bundesamts für Kartogr. und Geod., Frankfurt am Main, Germany, ISBN 3-89888-884-3.

McClusky, S., et al. (2000), GPS constraints on plate kinematics and dynamics in the eastern Mediterranean and Caucasus, *J. Geophys. Res.*, *105*, 5695–5719.

McClusky, S., R. Reilinger, S. Mahmoud, D. Ben Sari, and A. Tealeb (2003), GPS constraints on Africa (Nubia) and Arabia plate motions, *Geophys. J. Int.*, *155*, 126–138.

McKenzie, D., and J. Jackson (1986), A block model of distributed deformation by faulting, *J. Geol. Soc. London*, *143*, 349–353.

McKenzie, D., and J. Jackson (1989), The kinematics and dynamics of distributed deformation, in *Paleomagnetic Rotations and Continental Deformation*, edited by C. Kissel and C. Laj, pp. 17–31, Kluwer Acad., Dordrecht, Netherlands.

Paulsen, T., and T. Wilson (2004), Subglacial bedrock structure in the Transantarctic Mountains and its influence on the ice sheet flow: insight from RADARSAT SAR imagery, *Global Planet. Change*, *42*, 227–240.

Reading, A. M. (2002), Antarctic seismicity and neotectonics, in *Antarctica at the Close of a Millenium: Proceedings Volume, 8th International Sym-*

posium on Antarctic Earth Sciences, edited by J. A. Gamble et al., *R. Soc. N. Z. Bull.*, *35*, 479–484.
Reilinger, R., et al. (2006), GPS constraints on continental deformation in the Africa-Arabia-Eurasia continental collision zone and implications for the dynamics of plate interactions, *J. Geophys. Res.*, *111*, B05411, doi:10.1029/2005JB004051.
Ricci, C. A., F. Talarico, R. Palmeri, G. Di Vincenzo, and P. C. Pertusati (1996), Eclogite at the Antarctic palaeo-Pacific active margin of Gondwana (Lanterman Range, northern Victoria Land, Antarctica), *Antarct. Sci.*, *8*, 277–280.
Roland, N. W., and F. Tessensohn (1987), Rennick faulting—An early phase of Ross Sea rifting, *Geol. Jahrb. Reihe B*, *66*, 203–229.
Rossetti, F., F. Lisker, F. Storti, and A. Läufer (2003), Tectonic and denudational history of the Rennick Graben (North Victoria Land): Implications for the evolution of rifting between East and West Antarctica, *Tectonics*, *22*(2), 1016, doi:10.1029/2002TC001416.
Saastamoinen, J. (1972), Contributions to the theory of atmospheric refraction, *Bull. Geod.*, *105*, 279–298.
Salvini, F., and F. Storti (1999), Cenozoic tectonic lineaments of the Terra Nova Bay region, Ross Embayment, Antarctica, *Global Planet. Change*, *23*, 129–144.
Salvini, F., G. Brancolini, M. Busetti, F. Storti, F. Mazzarini, and F. Coren (1997), Cenozoic geodynamics of the Ross Sea region, Antarctica: crustal extension, intraplate strike-slip faulting, and tectonic inheritance, *J. Geophys. Res.*, *102*(24), 669–696.
Serpelloni, E., G. Casula, A. Galvani, M. Anzidei, and P. Baldi (2006), Data analysis of permanent GPS networks in Italy and surrounding regions: Applications of a distributed processing approach, *Ann. Geophys.*, *49*(4–5), 897–928.
Skinner, D. N. B. (1987), Terra Nova Bay and the Deep Freeze Range—The southern allochtonous border of north Victoria Land, Antarctica, *Mem. Soc. Geol. Ital.*, *33*, 41–58.
Storti, F., F. Rossetti, and F. Salvini (2001), Structural architecture and displacement accommodation mechanisms at the termination of the Priestly Fault, northern Victoria Land, Antarctica, *Tectonophysics*, *341*, 141–161.
Storti, F., F. Salvini, F. Rossetti, and J. P. Morgan (2007), Intraplate termination of transform faulting within the Antarctic continent, *Earth Planet. Sci. Lett.*, *260*, 115–126.
Turcotte, D. L., and G. Schubert (2002), *Geodynamics*, 2nd ed., 456 pp., Cambridge Univ. Press, Cambridge, U. K.
Weaver, S. D., J. D. Bradshaw, and M. G. Laird (1984), Geochemistry of Cambrian volcanics in northern Victoria Land, Antarctica, *Earth Planet. Sci. Lett.*, *68*, 128–140.
Wessel, P., and W. H. F. Smith (1998), New, improved version of Generic Mapping Tools released, *Eos Trans. AGU*, *79*(47), 579–583.
Williams, S. D. P. (2003), The effect of colored noise on the uncertainties of rates estimated from geodetic time series, *J. Geod.*, *76*(9–10), 483–494.
Williams, S. D. P. (2008), CATS: GPS coordinates time series analysis software, *GPS Solut.*, *12*, 147–153.
Willis, M., T. Wilson, and L. Hothem (2006), A decade of GPS measurements over the TAMDEF network, Victoria Land, Antarctica, European Geosciences Union, Vienna, 2–7 April 2006, *Geophys. Res. Abstr.*, *8*.
Wilson, J. T. (1965), A new class of faults and their bearing on continental drift, *Nature*, *207*, 363–367.
Wilson, T. J. (1995), Cenozoic transtension along the Transantarctic Mountains–West Antarctic rift boundary, southern Victoria Land, Antarctica, *Tectonics*, *14*, 531–545.
Wilson, T. J. (1999), Cenozoic structural segmentation of the Transantarctic Mountains rift flank in southern Victoria Land, *Global Planet. Change*, *23*, 105–127.
Wright, T. O., R. J. Ross Jr., and J. E. Repetski (1984), Newly discovered youngest Cambrian or oldest Ordovician fossils from the Robertson Bay Terrane (formerly Precambrian), northern Victoria Land, Antarctica, *Geology*, *12*, 301–305.
Zanutta, A., L. Vittuari, and S. Gandolfi (2008), Geodetic GPS-based analysis of recent crustal motions in Victoria Land (Antarctica), *Global Planet. Change*, *62*, 115–131.

A. Capra, Dipartimento di Ingegneria Meccanica e Civile, Università di Modena e Reggio dell'Emilia, Via Vignolese 905, I-41100 Modena, Italy.
G. Casula, Istituto Nazionale di Geofisica e Vulcanologia, Sezione di Bologna, Via D. Creti 12, I-40128 Bologna, Italy.
P. Cianfarra and F. Salvini, Dipartimento di Scienze Geologiche, Università degli Studi di Roma Tre, L.go S. L. Murialdo 1, I-00146 Roma, Italy. (cianfarr@uniroma3.it)
M. Dubbini, Dipartimento di Discipline Storiche, Antropologiche e Geografiche, Università di Bologna, Piazza San Giovanni in Monte 2, I-40124 Bologna, Italy.